Available online at www.sciencedirect.com
ScienceDirect
Journal of Computational Physics 227 (2008) 4589–4599
JOURNAL OF COMPUTATIONAL PHYSICS
www.elsevier.com/locate/jcp

Accurate method for including solid–fluid boundary interactions in mesoscopic model fluids

A. Berkenbos *, C.P. Lowe

Van't Hoff Institute for Molecular Sciences, Universiteit van Amsterdam, Nieuwe Achtergracht 166, 1018 WV Amsterdam, The Netherlands

Received 17 July 2007; received in revised form 7 January 2008; accepted 10 January 2008
Available online 26 January 2008

Abstract

Particle models are attractive methods for simulating the dynamics of complex mesoscopic fluids. Many practical applications of this methodology involve flow through a solid geometry. As the system is modeled using particles whose positions move continuously in space, one might expect that implementing the correct stick boundary condition exactly at the solid–fluid interface is straightforward. After all, unlike discrete methods there is no mapping onto a grid to contend with. In this article we describe a method that, for axisymmetric flows, imposes both the no-slip condition and continuity of stress at the interface. We show that the new method then accurately reproduces correct hydrodynamic behavior right up to the location of the interface. As such, computed flow profiles are correct even using a relatively small number of particles to model the fluid.

PACS: 02.70.−c; 47.11.−j; 47.15.Cb

Keywords: Complex fluid; Boundary conditions; Solid walls; Particle models

1. Introduction

Simulating the dynamics of mesoscopic fluids is a computational challenge. Mesoscopic systems contain particles that are large enough for external (hydrodynamic) forces to influence their dynamics but not so large that thermal (Brownian) forces are negligible. Classic examples are polymer solutions and colloidal suspensions. Simulating such fluids consequently requires accounting for both hydrodynamic and thermal effects. This is difficult using standard computational fluid dynamics methods. These normally work on a macroscopic scale, where thermal forces are negligible. The complexity of the fluid is then accounted for in terms of deviations from Newtonian fluid behavior as a result of the meso-scale effects. There is, however, considerable

* Corresponding author. Tel.: +31 20 525 6952; fax: +31 20 525 5604.
E-mail address: berkenbos@science.uva.nl (A. Berkenbos).

0021-9991/$ - see front matter © 2008 Elsevier Inc. All rights reserved.
doi:10.1016/j.jcp.2008.01.011

interest in developing methods that include both effects directly, thus avoiding treating the meso-scale in an *ad hoc* manner.

Several notable approaches have been developed to tackle this problem. In the Lattice–Boltzmann method (LB) one solves a fluctuating Boltzmann equation for a set of particles moving in discrete time with discrete velocities. The correct hydrodynamic behavior follows from the Chapman–Enskog expansion of hydrodynamic variables in terms of the microscopic evolution of the particle distribution functions. Thermal effects are introduced through statistical fluctuations in the stress tensor [1–5].

Alternatively, several methods explicitly model the fluid using particles moving continuously in space and interacting by some given rule. Two examples are dissipative particle dynamics (DPD) and stochastic rotational dynamics (SRD). In DPD, particles interact via three forces: a dissipative friction force between particles with different velocities, a conservative force in the form of a soft repulsive potential between the particles and a random force that maintains a correct thermodynamic equilibrium [6,7]. In the second example, SRD, the system is partitioned into cells at each time-step. The particles inside each cell exchange momentum by rotating their velocity around the center-off-mass velocity [8–10]. To enforce Galilean invariance, each time-step the position of the cells must undergo a random shift [11].

In both cases the interactions governing the evolution of the system satisfy the conditions required to reproduce correct hydrodynamic behavior (conservation of momentum, Galilean invariance and isotropy). Further, the interactions are specified in such a way that the equilibrium distribution is a thermodynamically defined statistical ensemble (canonical in the case of DPD, micro-canonical in the case of SRD). One drawback of these methods is that, unlike LB where the parameters can be varied almost at will, there is little freedom to vary the parameters [12,13]. Only for carefully chosen sets of parameters can the model fluid satisfy the conditions for realistic fluid dynamics [14]. However, they also have two notable advantages; firstly, a well defined thermodynamic equilibrium and secondly, the particles move continuously in space.

The reason one might expect that representing the fluid with a system that is continuous in space is advantageous is as follows. A large class of practically important problems in this field involve the flow of complex fluids through some solid geometry, polymer solutions in porous media for example. This requires simulating realistically the interaction of the fluid with a fixed solid phase. Specifically, imposing a "stick" boundary condition such that the fluid velocity at the interface is zero. In LB a simple bounce-back rule often suffices. This involves reversing the velocity of particles that would otherwise cross the interface. Identifying when this is the case involves discretizing the solid–fluid interface [15]. More sophisticated methods have been developed to generate a more continuous mapping of the surface to the lattice at the cost of greater computational complexity [16–20]. To some extent this problem is inevitable with LB because it solves a discretized equation. Mapping a continuous interface on a discrete solution is a generic difficulty in finite difference schemes. Using a particle model, there is no such discretization.

The off-lattice analogue of the bounce-back rule used in lattice Boltzmann, a particle undergoing velocity reversal when it impinges on the surface, guarantees that the average fluid velocity at the interface is zero. This way a stick boundary is recovered. One would therefore hope that it is possible to accurately represent the interface in continuous space. Unfortunately this is not the case. Firstly, if there are conservative interactions between the particles (as there usually are in DPD), these give rise to density fluctuation near to the interface. In turn, the transport coefficients are spatially dependent, inducing spurious effects near the boundary. It is possible to minimize these effects, by using an interface-particle potential that tries to maintain a uniform density, but not eliminate them completely [21–24]. One particularly elegant approach for square or cubic geometries is described by Visser et al. [25].

From a purely hydrodynamic point of view these conservative interactions are unnecessary. If there are no conservative interactions, the model solvent has an ideal gas equation of state. Examples of these types of methods are SRD and the dissipative ideal gas (DPD without conservative interactions) [26]. Both have been used successfully to study the dynamics of mesoscopic systems [13,27]. However, even in this case, where introducing a hard wall generates no density variations, a simple bounce-back rule is still inadequate. This is because for both methods momentum is transported by interactions between particles located within some pre-defined cut-off radius r_c of each other. To avoid introducing a spatially varying viscosity, particles in the vicinity of an interface should experience the same environment as particles in the bulk. This is exactly the reason that a "dummy region" of the same fluid, of width at least r_c, is required on the other side of

the boundary. The question is then, how should this dummy region be treated? One approach is to simply say it is filled with a fluid moving with zero velocity (i.e. the velocity of the interface itself) [28,29]. However, in this article we show that for axisymmetric flows the dummy region can be treated such that the stress is continuous across the interface. This method is more accurate, particularly when the number of particles used to model the solvent is relatively low.

2. Description of the method

While we could use SRD or a dissipative ideal gas, here we choose to use a method closely related to the latter, namely an ideal gas coupled to a Lowe–Andersen (LA) thermostat [30]. This method is similar in spirit to the dissipative ideal gas. There are three reasons why we use it here. First, it satisfies semi-detailed balance, so the equilibrium properties are correct even for long time-steps [31,32]. Consequently, we do not have to worry about density variations introduced as artifacts of integrating the equations of motion numerically. Second, in this system particles undergo ballistic motion for a time-step Δt followed by impulsive collisions. This means that it is possible to compute exactly the trajectory of particles that collide with the interface because during one time-step their motion is deterministic. Third, the equilibrium distribution is canonical so there is no need for an additional thermostat.

The method works as follows. Each time-step, all pairs of particles within a distance r_c of each other have a probability of undergoing a "virtual" collision. Such a collision involves generating a new relative velocity from the Maxwell–Boltzmann distribution along the line of centers of the two particles. This operation is carried out in such a way that linear momentum is conserved. Because the force only acts along the line of centers, collisions also conserve angular momentum. Additionally, only relative velocities are involved, so the LA thermostat is Galilean invariant. These properties ensure we obtain correct hydrodynamic behavior, on sufficiently long time and length scales [30]. Despite the fact we effectively use an ideal gas solvent, we can still recover realistic solvent behavior so long as we choose the model parameters with care. There is a limited parameter space where one can reasonably argue that an ideal gas model solvent has liquid-like behavior, and here we restrict ourselves to this regime [13].

Our basic requirements at the interface are the following. Firstly that we recover a stick boundary. That is, the average flow velocity at the boundary should be zero. Secondly, the presence of the interface does not perturb the transport properties of the solvent. The first condition is straightforward to enforce. We use a "bounce-back" rule, meaning that the direction of the velocity of particles that impinge on the interface is reversed. Specifically, positions $\mathbf{r}$ and velocities $\mathbf{v}$ of particles that collide with the interface during a time-step Δt are update according to:

$$\mathbf{r}(t+\Delta t) = \mathbf{r}(t) + 2\mathbf{v}(t)\tau_c - \mathbf{v}(t)\Delta t, \tag{1}$$

$$\mathbf{v}(t+\Delta t) = -\mathbf{v}(t), \tag{2}$$

where τ_c is the time elapsed from the start of the time-step to the occurrence of an interface collision. Under this operation the average of the pre- and post-interface collision velocity of the particles is zero, so in this sense it always enforces a stick boundary. To enforce the second condition, we follow other workers and introduce a "dummy" region [33–39]. This is a region of minimum width r_c that contains a fluid that is identical to the fluid in the real system (all parameters, including the density, are equal). The interface between the dummy region and the real system we term the "real interface" (the dummy region is simply a device to ensure that the real interface behaves correctly). Interactions between the system particles and dummy particles are evaluated in the normal way: there is no difference between particle types. This means that a fluid particle located at the real interface experiences the same environment as a particle in the bulk, eliminating the problem of having a spatially varying viscosity in the region of the interface. Because the particle fluid has an ideal gas equation of state, the interface will not generate density variations in the model fluid.

The question is now, how do we treat the fluid particles in the dummy region? We begin by considering the force the model fluid exerts on the interface for the simplest case: the flow of a fluid between two infinite parallel plates. The force density $\widetilde{F}_s(\mathbf{r})$ exerted by a Newtonian fluid on a surface, with normal vector $\hat{\mathbf{n}}$ directed from the boundary towards the fluid, is given by

$$\widetilde{F}_s(\mathbf{r}) = \boldsymbol{\tau} \cdot \hat{\mathbf{n}}, \tag{3}$$

where the stress tensor $\boldsymbol{\tau}$ for a fluid with shear viscosity η at a pressure p is given by

$$\tau_{ij} = p\delta_{ij} + \eta\left(\frac{\partial v_i}{\partial r_j} + \frac{\partial v_j}{\partial r_i}\right), \tag{4}$$

where v_i is the i component of the local flow velocity. Let us consider the force on the surface of one plate occupying the $z = 0$ plane due to a flow in the x direction on the"system side" ($z > 0$):

$$F_x^S = \int_S \eta \frac{\partial v_x}{\partial z}\bigg]_{0^+} \mathrm{d}s. \tag{5}$$

Here, the superscript + indicates that the derivative is evaluated on the system side of the interface. On the other hand, the force due to a flow in the x direction on the "dummy side" of the plate is

$$F_x^D = -\int_S \eta \frac{\partial v_x}{\partial z}\bigg]_{0^-} \mathrm{d}s \tag{6}$$

If we can arrange for these two forces to be equal and opposite, $F_x^S + F_x^D = 0$, then, because all points on the surface are equivalent, it follows that

$$\frac{\partial v_x}{\partial z}\bigg]_{0^+} = \frac{\partial v_x}{\partial z}\bigg]_{0^-}. \tag{7}$$

That is, the stress will be continuous across the interface. We should also point out that the same argument applies for a cylindrical tube because in cylindrical coordinates the axial component of the fluid velocity behaves in the same way with respect to the direction normal to the surface (in this case the radial direction simply replaces the z direction). Because of the radial symmetry it again follows that the stress will be continuous.

To summarize, if we can impose the condition that the average total force exerted on the interface by the real system and dummy region is zero, it follows that the stress across the interface is continuous. To satisfy this we adopt the following procedure, illustrated diagrammatically in Fig. 1. The dummy system and the real system are separated by a no-slip boundary, so the bounce-back rule is applied for both particles in the real and dummy regions when they impinge on this interface. To complete the system we confine the particles in the dummy region with a second hard wall. Since particles cannot cross either boundary, dummy particles are always dummy particles and the number of particles in each region is constant. The important point now is

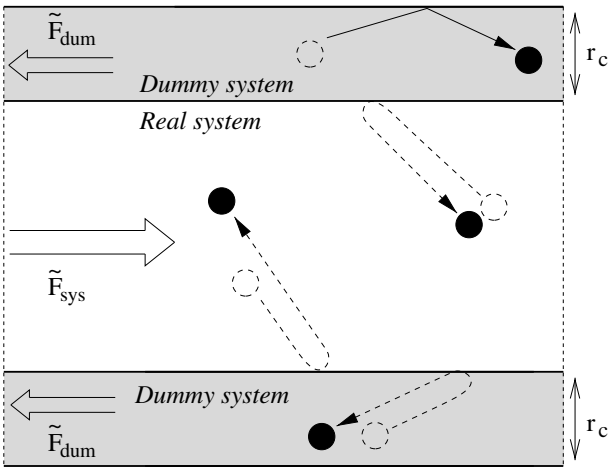

Fig. 1. Schematic overview of the boundary method described in this article. The circles represent the solvent particles and the small arrows show how they collide with the interface. The "real" interface between the system region and the dummy region is a no-slip boundary. The dummy region is confined by slip boundaries.

that for the interface that confines the dummy region, we use a "bounce-forward" rule. That is, the positions and velocities of dummy particles that impinge on the confining boundary are updated according to

$$\mathbf{r}(t+\Delta t) = \mathbf{r}(t) + \mathbf{v}_{\parallel}(t)\Delta t + 2\mathbf{v}_{\perp}(t)\tau_c - \mathbf{v}_{\perp}(t)\Delta t, \tag{8}$$

$$\mathbf{v}(t+\Delta t) = \mathbf{v}_{\parallel}(t) - \mathbf{v}_{\perp}(t), \tag{9}$$

where $\mathbf{v}_{\parallel}(t)$ and $\mathbf{v}_{\perp}(t)$ are the components of the velocity parallel and perpendicular to the interface, respectively. This operation does not change the momentum in the axial direction (it imposes a slip boundary condition). The force on this interface is therefore zero, so the total force acting on the fluid is only the sum of the force exerted on the two sides of the real interface. Now, if we ensure that the total external force acting on the system itself is zero, it follows that Eq. (7) will be satisfied and the stress should be continuous across this interface. This is straightforward to arrange. An external force density $\widetilde{F}_{\mathrm{sys}}$ acting in the axial direction is required to drive the flow in the real system. This force only acts on particles in the real system. The condition of no total force now simply requires that we apply an external force density to the fluid in the dummy region, $\widetilde{F}_{\mathrm{dum}}$, such that

$$\widetilde{F}_{\mathrm{dum}} = -\widetilde{F}_{\mathrm{sys}} \frac{V_{\mathrm{sys}}}{V_{\mathrm{dum}}}. \tag{10}$$

In summary, by using a slip condition on the interface that confines the dummy region we know that the total force acting on the system is balanced by the force on the real interface. If we ensure that the total force applied to the system is zero, then this force must be zero as well. Consequently, the force on the two sides of the real interface is equal and opposite, implying continuity of the stress. Again, this should hold for both planar and tubular geometries.

3. Results

Using the methodology described above, we have calculated velocity profiles for two systems. The first system we consider is flow through a cylindrical tube. As noted, for this system we expect the stress to be continuous across the real interface. Secondly, we consider flow through a tube with an elliptical cross-section. The argument above does not necessarily hold for this case, because there is no radial symmetry. We therefore use it as test case for more general axisymmetric flows.

For a detailed comparison with theoretical results, an accurate value for the viscosity of the fluid is required. We calculated this in separate simulations of a bulk fluid using the Poiseuille method [40]. In the case of a confined fluid there is an additional Knudsen-like parameter Λ, defined as the ratio of the typical fluid particle separation ($1/\rho^{1/3}$, where ρ is the number density) to the typical geometry width L, $\Lambda = 1/(L\rho^{1/3})$. This is effectively the degree of resolution of the model solvent, the analogue of the grid spacing in a finite difference method. Note that the larger the value of Λ, the fewer solvent particles are required to model the solvent. This means that the simulations are proportionately less computationally demanding. For the tubular geometry we take the characteristic length L, as being the tube radius R and for the ellipse, the length of the minor axis β. The external force acting on the fluid in the real system and dummy system regions were applied by adding additional momentum in the axial direction after the collision step of the LA thermostat, such that the requirement in Eq. (10) holds. In all cases this force was chosen such, that the Reynolds number ($Re = \rho V_0 L/\eta$, where V_0 is the maximum flow velocity) was significantly less than unity. Therefore the results apply for the creeping flow regime, which is characteristic for the microscopic scale.

In Figs. 2 and 3 we plot the axial flow velocity field $V(r)$, where r is the distance from the center, calculated for values $\Lambda = 0.100$ and $\Lambda = 0.041$, respectively. The velocity fields were calculated by time-averaging the spatial velocity in small sub-volumes, after the systems reached the steady state (that is, once these averages were independent of time). This procedure is necessary for a mesoscopic model fluid because the thermal motion of the solvent particles is not negligible. In the figures, the velocity is normalized by the theoretical maximum flow velocity [41]:

$$V_0 = \frac{\widetilde{F}_{\mathrm{sys}} R^2}{4\eta}. \tag{11}$$

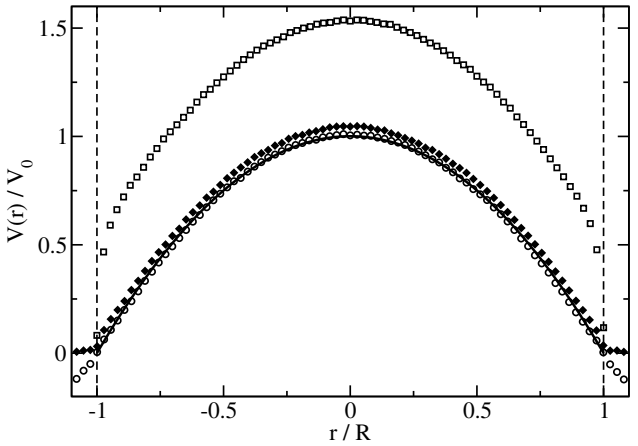

Fig. 2. Velocity profile for three different boundary methods. The open squares represent the "no dummy" method, the filled diamonds represent the "random dummy" method and the open circles represent the "new method". The solid line follows the exact solution given by Eq. 12. The vertical dotted lines show the position of the real interface. In this case $\Lambda = 0.100$.

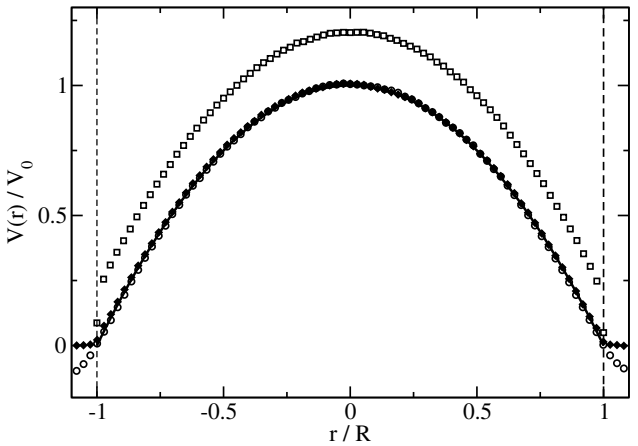

Fig. 3. Velocity profile for three different boundary methods. The open squares represent the "no dummy" method, the filled diamonds represent the "random dummy" method and the open circles represent the "new method". The solid line follows the exact solution given by Eq. 12. The vertical dotted lines show the position of the real interface. In this case $\Lambda = 0.041$.

We have calculated these data using three methods for implementing the solid–fluid interface:

- "New method", as described above;
- "no dummy", a system without a dummy region and a bounce-back rule at the system boundary;
- "random dummy", a system with a dummy region and a bounce-back rule at the interface of the system and dummy region. At the end of each time-step the velocity of the fluid particles in the dummy region is generated randomly from the distribution of thermal velocities at zero flow velocity [28,29].

Also plotted is the exact result (valid in the limit $Re \ll 1$) [41]:

$$\frac{V(r)}{V_0} = \left[1 - \left(\frac{r}{R}\right)^2\right]. \tag{12}$$

As the plots show, without using a dummy region the results are poor. Deviations of the flow velocity from the exact result are pronounced for both values of Λ. The agreement is better for the lower value of Λ (higher

resolution), suggesting that the correct profile is at least recovered in the limit $\Lambda \to 0$. For the "random dummy" method, the results for the lower value of Λ are much better, and do not differ significantly from the exact profile on the scale of the figure. However, for the higher value there is a small but significant difference. Finally, for the "new method" there are no significant deviations, for both values of Λ. In the figure we show the velocity field in both the real system and dummy region (the interface is marked with the dashed line). As we expect, for the new method, this is continuous across the interface.

To examine more carefully the accuracy of these methods near the boundary itself, in Fig. 4 we show the velocity fields in this region for $\Lambda = 0.041$. Here, the average local flow velocities are calculated on a finer spatial scale. As the figure shows, without the dummy region the velocity does in fact approach zero at the interface. That is, the bounce-back rule is indeed sufficient to enforce this condition. Unfortunately, as the plots show, there is a severe boundary artifact close to the interface. Although it is not clear from Fig. 3, for the "random dummy" method, there is in fact a relatively small but observable error. In contrast, using the new method, the velocity is exact right up to the interface in both cases. It is possible to quantify the deviations from exact behavior near the interface by determining a "slip length", l_s. We determined l_s by plotting the velocity profiles as a function of $(r/R)^2$, in which case the exact solution is linear. At the point where the calculated velocity starts to deviate from linearity, we extrapolate the original line to zero. This is the position where the "effective" boundary of the system is located. Now we define l_s as the difference between the position of the effective boundary and the actual boundary. In Fig. 5 we show how we determine $l_s \sim \sqrt{1.50 - 1.00} = 0.70$, in the case with no dummy region at $\Lambda = 0.100$. In Table 1 we have tabulated the results for l_s/R using the alternative boundary methods at three different resolutions, the two illustrated in Figs. 2 and 3 ($\Lambda = 0.100$ and 0.041) and a higher value for $\Lambda = 0.149$.

For both alternative methods, l_s decreases with decreasing Λ. In the biggest system the random dummy method has a slip length of only 3% of the tube diameter. Using the same procedure, the new method gives a slip length statistically indistinguishable from zero for all three cases.

Finally we turn to the case of a tube which lacks axial symmetry: an elliptical cross-sectional geometry. As noted above, the argument that our method ensures that the stress is continuous at the interface does not necessarily hold for this system. In this specific example we set the ratio of the major axis (α) to the minor axis β to be $\alpha/\beta = 2.0$. We specify $\Lambda = 0.2$, taking the minor axis β as the characteristic length L. In Fig. 6 the results for the velocity profile along the major and minor axis are plotted. The theoretical expression for the flow velocity in tubes with an elliptic cross-section at $Re \to 0$, is given by the following expression [42]:

$$\frac{V(\mathbf{r})}{V_0} = \left(1 - \frac{x^2}{\alpha^2} - \frac{y^2}{\beta^2}\right). \tag{13}$$

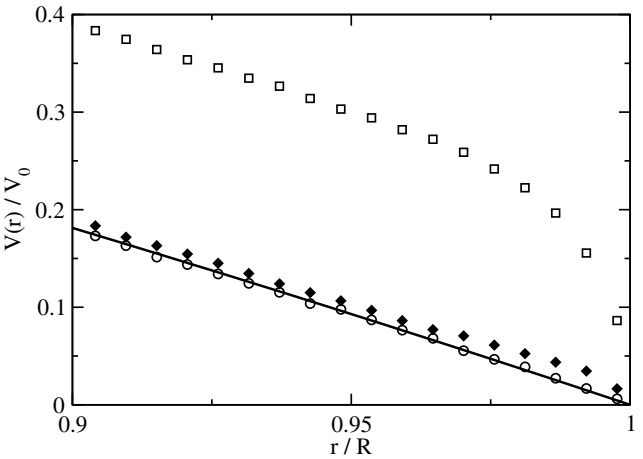

Fig. 4. Close up of the velocity profile of Fig. 3 near one boundary. The open squares represent the "no dummy" method, the filled diamonds represent the "random dummy" method and the open circles represent the "new method". The solid line follows the exact solution given by Eq. 12. In this case $\Lambda = 0.041$.

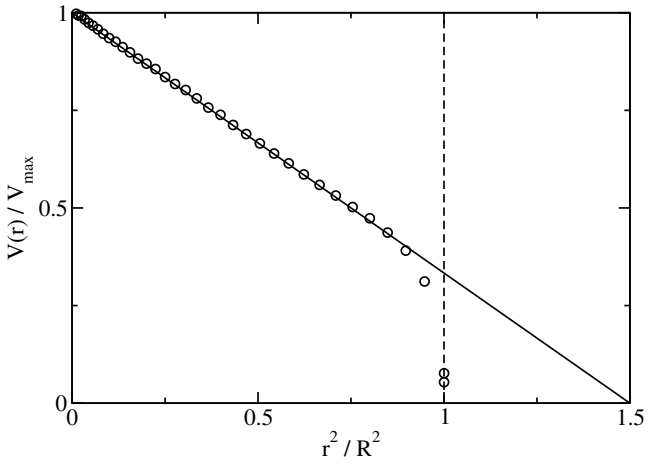

Fig. 5. Illustration of how the slip length l_s is determined. The circles represent the average velocity of a solvent in a tube, simulated with the "no dummy" method and $\Lambda = 0.100$. The exact results should be a straight line through the position of the interface at $x^2 = 1.00$. The dotted line illustrates how we extrapolate to determine l_s, here $l_s \sim \sqrt{1.50 - 1.00} = 0.70$.

Table 1
Measured slip lengths l_s, at three different values for Λ, for the two alternative boundary methods

Λ	l_s/R no dummy	l_s/R random dummy
0.149	0.8	0.3
0.100	0.7	0.2
0.041	0.4	0.06

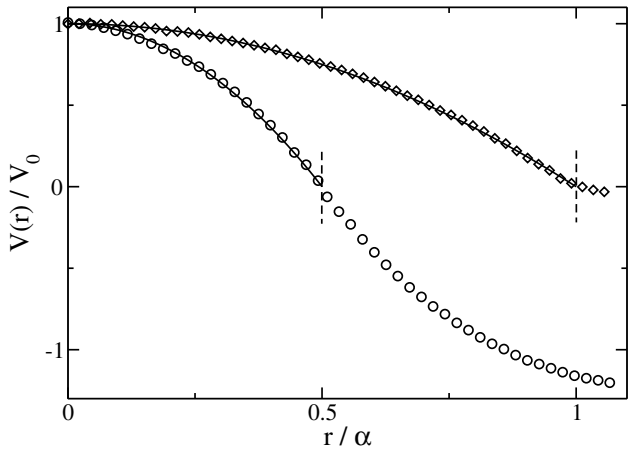

Fig. 6. Velocity profile for the new boundary method in a tube with an elliptical cross-section. The ratio of the major axis (α) to the minor axis (β) is $\alpha/\beta = 2.0$. Here, $\Lambda = 0.2$. The diamonds represent the velocity along the α axis, the circles the velocity along the β axis. The solid lines follow the exact solution given by Eq. (13). The vertical dotted lines are the positions of the solid–fluid interface.

There is excellent agreement between the flow profile in Fig. 6 and the theoretical expression in Eq. (13). Furthermore, as the plot shows the stress is again continuous across the interface.

4. Conclusions

All three methods we have considered in this article impose the correct stick boundary condition at the solid–fluid interface. They only differ in how accurately they reproduce the flow profile for a given degree of coarseness of the model solvent (as measured by Λ). Without a dummy region, there is a pronounced boundary layer near the interface, with a width roughly equal to the particle interaction radius. This method will only work adequately, even far from the interface, for extremely small values of Λ. Using a dummy region within which the velocities are constrained to have a thermal velocity, but no flow velocity, is a vast improvement. For small values of Λ the profile agrees reasonably well with the exact solution. However, there is always a small error near the boundary and for larger values of Λ this leads to significant errors, even far from the interface. The method we have described for implementing a solid–fluid interface ensures that the stress is continuous across the interface. For all the values of Λ we have studied, the flow velocity agrees precisely (to the accuracy we have calculated it) with the exact values, over the whole system. Furthermore, while we only justified the method for the axisymmetric case, the method works equally well for a system that does not have this symmetry (an elliptical cross-section). For both cases we restricted testing our methodology to the low Reynolds number regime. However, so long as the flow is non-linearly stable the physical reasoning behind the method still holds. That is, it should be valid even at non-negligible Reynolds numbers, much higher than those studied here.

Clearly, the important difference between the methods is how well they perform at larger values of Λ. That is, where the fluid is represented with a relatively small number of particles. The method we describe here is always the most accurate. One could reasonably argue that the "random dummy" method is adequate for most purposes, so long as Λ is not too large. However, since small values of Λ require a proportionately larger number of solvent particles to resolve the fluid, using larger values (as the new method allows) significantly reduces the amount of computation. This also has consequences when one considers using these kind of methods to study "real" complex fluids, not just the solvent [43]. Considering polymer solutions, to accurately capture the hydrodynamics, the typical distance between beads in the model polymer must be similar to the solvent interparticle separation [13]. This means that smaller values of Λ require longer model polymers, when the ratio of the polymer size to the tube width is fixed. Again, this is computationally inconvenient. As a caveat, we should also add that the introduction of a dummy region itself introduces some computational overhead because the simulated system is bigger than strictly necessary. This overhead, compared to a (hypothetical) method that does not use a dummy region, scales as $2r_c/R + (r_c/R)^2$, so it is only significant if $r_c \sim R$. In practice this is of little concern because one only expects to recover hydrodynamic behavior for the model solvent on length scales greater than r_c. This requires that $R > r_c$ for the methodology to be reliable.

The fluid itself was modeled using an ideal gas coupled to a LA-thermostat. However, this is something of a matter of taste. Because the method is physically based, it could equally well be applied to any of the other particle techniques that use a system with an ideal gas equation of state (SRD or a dissipative ideal gas for example). Here we have restricted ourselves to geometries with a cross-section that is independent of axial position. The method could in principle be extended to more complex geometries but in this case it is not *a priori* obvious that it will be more accurate than the "random dummy" method. Nonetheless, it would be interesting to test this hypothesis.

To summarize, we have developed a method that accurately models the interaction between a particle model fluid and a fixed solid boundary. We demonstrated that the method is advantageous for an important set of problems. Specifically, axial flow through a geometry with a constant cross-section. Its advantages are two-fold: it introduces no boundary artifacts and allows one to accurately model the flow with a relatively small number of solvent particles. The latter reduces the amount of computational work required to solve a given problem. As such, we hope that it will be a useful addition to the mesoscopic simulators armory.

Acknowledgment

The authors acknowledge the Nederlandse Organisatie voor Wetenschappelijk Onderzoek (NWO) for financial support.

References

[1] G. McNamara, B. Alder, Use of the Boltzmann equations to simulate lattice-gas automata, Phys. Rev. Lett. 61 (1988) 2332.
[2] S. Chen, Z. Wang, X. Shan, G. Doolen, Lattice Boltzmann computational fluid dynamics in three dimensions, J. Statist. Phys. 68 (1992) 379.
[3] A. Ladd, Numerical simulations of particulate suspensions via a discretized Boltzmann equation. Part 1. Theoretical foundation, J. Fluid Mech. 271 (1994) 285.
[4] A. Ladd, Numerical simulations of particulate suspensions via a discretized Boltzmann equation. Part 2. Numerical results, J. Fluid Mech. 271 (1994) 311.
[5] R. Adhikari, K. Stratford, M.E. Cates, A.J. Wagner, Fluctuating Lattice Boltzmann, Europhys. Lett. 71 (2005) 473.
[6] P. Hoogerbrugge, J. Koelman, Simulating microscopic hydrodynamic phenomena with dissipative particle dynamics, Europhys. Lett. 19 (1992) 155.
[7] P. Español, P. Warren, Statistical-mechanics of dissipative particle dynamics, Europhys. Lett. 30 (1995) 191.
[8] A. Malevanets, R. Kapral, Mesoscopic model for solvent dynamics, J. Chem. Phys. 110 (1999) 8605.
[9] A. Malevanets, R. Kapral, Solute molecular dynamics in a mesoscale solvent, J. Chem. Phys. 112 (2000) 7260.
[10] N. Kikuchi, C. Pooley, J. Ryder, J. Yeomans, Transport coefficients of a mesoscopic fluid dynamics model, J. Chem. Phys. 119 (2003) 6388.
[11] T. Ihle, D. Kroll, Stochastic rotation dynamics: a Galilean-invariant mesoscopic model for fluid flow, Phys. Rev. E 63 (2001) 020201.
[12] J. Padding, A. Louis, Hydrodynamic interactions and Brownian forces in colloidal suspensions: coarse-graining over time and length scales, Phys. Rev. E 74 (2006) 031402.
[13] C.P. Lowe, A.F. Bakker, M.W. Dreischor, The influence of time-dependent hydrodynamics on polymer centre-of-mass motion, Europhys. Lett. 67 (2004) 397.
[14] C.P. Lowe, M.W. Dreischor, Simulating the dynamics of mesoscopic systems, Lect. Notes Phys. 640 (2004) 39.
[15] D. Kandhai, A. Koponen, A. Hoekstra, M. Kataja, J. Timonen, P. Sloot, Implementation aspects of 3D Lattice-BGK: boundaries, accuracy, and a new fast relaxation method, J. Comp. Phys. 150 (1999) 482.
[16] D. Ziegler, Boundary conditions for lattice Boltzmann simulations, J. Stat. Phys. 71 (1993) 1171.
[17] P. Skordos, Initial and boundary condition for the lattice Boltzmann method, Phys. Rev. E 48 (1993) 4823.
[18] D. Noble, S. Chen, J. Georgiadis, R. Buckius, A consistent hydrodynamic boundary condition for the lattice Boltzmann method, Phys. Fluids 7 (1995) 203.
[19] D. Noble, J. Georgiadis, R. Buckius, Comparison of accuracy and performance of lattice Boltzmann and finite difference simulations of steady viscous flow, Int. J. Numer. Methods Fluids 23 (1996) 1.
[20] S. Chen, D. Martinez, R. Mei, On boundary conditions in lattice Boltzmann methods, Phys. Fluids 8 (1996) 2527.
[21] D. Duong-Hong, N. Phan-Thien, X. Fan, An implementation of no-slip boundary conditions in DPD, Comput. Mech. 35 (2004) 24.
[22] I.V. Pivkin, G.E. Karniadakis, A new method to impose no-slip boundary conditions in dissipative particle dynamics, J. Comp. Phys. 207 (2005) 114.
[23] L.M. Wang, W. Ge, J.H. Li, A new wall boundary condition in particle methods, Comput. Phys. Commun. 174 (2006) 386.
[24] I.V. Pivkin, G.E. Karniadakis, Controlling density fluctuations in wall-bounded dissipative particle dynamics systems, Phys. Rev. Lett. 96 (2006) 206001.
[25] D. Visser, H. Hoefsloot, P. Iedema, Comprehensive boundary method for solid walls in dissipative particle dynamics, J. Comp. Phys. 205 (2005) 626.
[26] I. Pagonabarraga, M.H.J. Hagen, D. Frenkel, Self-consistent dissipative particle dynamics algorithm, Europhys. Lett. 42 (1998) 377.
[27] M. Ripoll, K. Mussawisade, R.G. Winkler, G. Gompper, Low-Reynolds-number hydrodynamics of complex fluids by multi-particle-collision dynamics, Europhys. Lett. 68 (2004) 106.
[28] A. Lamura, G. Gompper, T. Ihle, D.M. Kroll, Multi-particle collision dynamics: flow around a circular and a square cylinder, Europhys. Lett. 56 (2001) 319.
[29] N. Wataria, M. Makino, N. Kikuchi, R. Larson, M. Doi, Simulation of DNA motion in a microchannel using stochastic rotation dynamics, J. Chem. Phys. 126 (2007) 094902.
[30] C.P. Lowe, An alternative approach to dissipative particle dynamics, Europhys. Lett. 47 (1999) 145.
[31] P. Nikunen, M. Karttunen, I. Vattulainen, How would you integrate the equations of motion in dissipative particle dynamics simulations? Comput. Phys. Commun. 153 (2003) 407.
[32] A.F. Jakobsen, O.G. Mouritsen, G. Besold, Artifacts in dynamical simulations of coarse-grained model lipid bilayers, J. Chem. Phys. 122 (2005) 204901.
[33] Y. Kong, C. Manke, W. Madden, A. Schlijper, Simulation of a confined polymer in solution using the dissipative particle dynamics method, Int. J. Thermophys. 15 (1994) 1093.
[34] M. Revenga, I. Zuniga, P. Espanol, I. Pagonabarraga, Boundary models in DPD, Int. J. Mod. Phys. C 9 (1998) 1319.
[35] J. Jones, M. Lal, J. Ruddock, N. Spenley, Dynamics of a drop at a liquid/solid interface in simple shear fields: a mesoscopic simulation study, Faraday Discuss. 112 (1999) 129.
[36] M. Revenga, I. Zuniga, P. Espanol, Boundary conditions in dissipative particle dynamics, Comput. Phys. Commun. 122 (1999) 309.
[37] J. Gibson, K. Zhang, K. Chen, S. Chynoweth, C.W. Manke, Simulation of colloid-polymer systems using dissipative particle dynamics, Mol. Simulat. 23 (1999) 1.
[38] S.M. Willemsen, H.C.J. Hoefsloot, P.D. Iedema, No-slip boundary condition in dissipative particle dynamics, Int. J. Mod. Phys. C 11 (2000) 81.

[39] X. Fan, N. Phan-Thien, N. Yong, X. Wu, D. Xu, Microchannel flow of a macromolecular suspension, Phys. Fluids 15 (2003) 11.
[40] J.A. Backer, C.P. Lowe, H.C.J. Hoefsloot, P.D. Iedema, Poiseuille flow to measure the viscosity of particle model fluids, J. Chem. Phys. 122 (2005) 154503.
[41] R.B. Bird, W.E. Stewart, E.N. Lightfoot (Eds.), Transport Phenomena, Wiley and Sons, New York, 1960.
[42] M. Haslam, M. Zamir, Pulsatile flow in tubes of elliptic cross sections, Ann. Biomed. Eng. 26 (1998) 780.
[43] A. Berkenbos, C.P. Lowe, Mesoscopic simulations of accelerated polymer drift in microfluidic capillaries, J. Chem. Phys. 127 (2007) 164902.